Dynamics of methane molecules in porous TiO_2

2000 J. Phys.: Condens. Matter 12 1613

(http://iopscience.iop.org/0953-8984/12/8/304)

J. Phys.: Condens. Matter **12** (2000) 1613–1626. Printed in the UK PII: S0953-8984(00)05623-X

Dynamics of methane molecules in porous TiO_2

I A Krasnov†, B Asmussen†‖, C Gutt†, W Press†, W Langel‡ and M Ferrand§

† Institut für Experimentelle und Angewandte Physik, Universität Kiel, Olshausenstrasse 40, D-24098 Kiel, Germany

‡ Institut für Physikalische Chemie, Universität Greifswald, Soldtmannsstrasse 23, D-17487 Greifswald, Germany

§ Institut Laue–Langevin, BP 156X, F-38042 Grenoble Cédex, France

Received 30 June 1999, in final form 11 November 1999

Abstract. A neutron scattering study of the dynamics of CH_4 molecules in the restricted geometry of porous TiO_2 with an average pore diameter of 110 Å is presented. Two different coverages were studied: (1) completely filled pores; (2) walls covered by a monomolecular film. Rotational tunnelling spectra of the methane rotors at $T = 5$ K show the coexistence of the low-temperature phase of bulk methane (phase II) with a disordered phase (phase I′) in a layer close to the wall. In the melting region of the condensate, the neutron spectra yield information about translational and rotational motion of the methane molecules. The fraction $x(T)$ of molecules that are in the liquid phase increases over a rather wide temperature range from $x \sim 0$ at $T = 83$ K up to $x \sim 1$ at $T = 95$ K.

1. Introduction

Recently, porous materials have attracted considerable interest, and continue to do so. This is mainly for the following reasons:

(1) They bear enormous potential for technical applications (e.g. catalysis, where they are used in large quantities).
(2) They provide a framework for basic investigations of the physical properties of solids under the condition of a restricted geometry.

When materials are confined into small pores, their properties may change substantially. In particular, phase transitions can be strongly affected as result of finite-size effects of interactions between the guests and pore walls, and orientational and translational disorder introduced into the system by the guests.

The currently most extensively studied porous materials can be classified as either regular or irregular structures. Examples of the regular materials are the zeolites or MCM-41 [9]; the irregular materials are represented by e.g. Vycor glass or silica gel. Guest molecules of particular interest are e.g. hydrogen [18] (because of the possibility of observing superfluid behaviour, when confined to small pores) and H_2O, where special attention has been paid to the melting transition [10, 14]. In this paper we present a neutron scattering study of the dynamics of CH_4 molecules in the irregular framework of porous TiO_2 (pore diameters of the order of 110 Å). TiO_2 has considerable importance for technical applications, e.g. in catalysis and (photo)electrochemistry [6]. The motivation for selecting methane as guest molecule lies

‖ Author to whom any correspondence should be addressed.

0953-8984/00/081613+14$30.00

in its high symmetry. Two different loadings were investigated: (1) completely filled pores; and (2) pore walls covered by a thin film of CH_4 molecules (thickness $\sim$1 monolayer).

At low temperatures ($T \leqslant 10$ K) the rotational dynamics of the methane rotors gives rise to a specific inelastic scattering, which is a sensitive probe for local orientational order/disorder of the condensate. In an investigation of CH_4 in silica gels with several pore diameters ($d \leqslant 100$ Å) and also in MCM-41 (cylindrical pores with $d \sim 30$ Å) [11] we have found a broad distribution of local orientational potentials without any long-range orientational ordering of the guest molecules. The spectra were analysed in terms of a Gaussian distribution of the local potentials. This approach was extended in a study of the quantum rotations of methane molecules in two controlled-pore glasses (CPG) with average pore diameters of $d = 120$ Å and $d = 350$ Å [12], where the analysis was improved by taking into account the T-state splitting due to the low symmetry of the local potentials. The neutron spectra gave clear evidence for the formation of a core with the orientational ordering of CH_4-II in pores with $d \geqslant 120$ Å and an orientationally disordered layer of thickness $d \sim 15$ Å on the pore walls.

With increasing temperature, quasielastic scattering due to rotational diffusion of the CH_4 rotors occurs. Of particular interest is the melting of the condensates. The melting region is characterized by the onset of translational diffusion, causing a decrease of the self-correlation function $G_s(\vec{r}, t)$ for $t \to \infty$. This leads to a corresponding decrease of the elastic intensity with increasing temperature and, hence, makes the incoherent scattering a very sensitive tool for the investigation of the melting behaviour.

In the following section we describe the characterization of the sample by sorption isotherms and give the experimental details of the neutron scattering experiments. Section 3 is devoted to the neutron scattering experiments. The low-temperature (rotational) dynamics of the CH_4 molecules will be discussed in terms of a quantum-mechanical description, while the temperature range 50 K $\leqslant T \leqslant$ 100 K is characterized by rotational diffusion and the onset of translational diffusion near the condensate melting point. Section 4 focuses on the melting behaviour. Section 5 contains a summary and conclusions.

2. Sorption properties of the porous TiO_2

The porous TiO_2 was provided by Sachtleben Chemie GmbH, Duisburg. It is produced by a process of hydrolysis of titanium oxide hydrate and contains *primary particles* with typical linear dimensions of the order of several hundred ångströms. These primary particles are crystalline with anatase structure [4] (the anatase modification is less stable than the rutile modification of TiO_2, but is more widely used in catalysis) and aggregate to form larger *secondary particles* with spherical shape and diameters of about 1 μm. Small voids (mesopores) with diameters of $\sim$100 Å form between the primary particles, while larger cavities (macropores) occur between the secondary particles [16].

Measuring vapour-pressure isotherms is a standard method for characterizing the sorption behaviour of a porous host material. Figure 1(a) shows the CH_4 sorption/desorption isotherm of the TiO_2 sample. It was measured with 2.95 g TiO_2 at $T = 92$ K and is of type IV according to Brunauer's classification [2] with two characteristic regions:

- *Multilayer adsorption:* the slowly increasing part in the pressure range 10 mbar $\leqslant p \leqslant$ 70 mbar indicates the formation of a thin layer of methane on the inner surfaces of the sample.
- *Capillary condensation:* the strong increase of the adsorbed amount of gas for 70 mbar $\leqslant p \leqslant$ 125 mbar is due to complete filling of the mesopores. Adsorption and desorption take place at different pressures (hysteresis behaviour). In a very narrow pressure range around

$p \sim 130$ mbar (most clearly visible in the desorption branch), the isotherm levels off before the saturation pressure is reached because now all pores are filled with condensate.

Various ways for calculating the pore size distribution from a given sorption/desorption isotherm are described by Adamson in reference [1]. We have used the following procedure:

(1) For given temperature T and pressure p, a multilayer film of thickness $h(p)$ is formed. $h(p)$ may be calculated on the basis of the *Frenkel–Halsey–Hill model* (the FHH model) [1, 5]:

$$h(p) = h_m \left(\frac{\epsilon_0}{k_B T \ln(p_0/p)} \right)^{1/k}. \tag{1}$$

h_m is the thickness of the monolayer coverage and p_0 denotes the saturation vapour pressure of methane at temperature T. The energy ϵ_0 and the inverse exponent k characterize the interaction potential of the gas particle and the pore wall. $n(p)$, the number of adsorbed molecules, is related to $h(p)$ by

$$\frac{n(p)}{n_m} = \frac{h(p)}{h_m}. \tag{2}$$

n_m is the number of molecules needed to form the monolayer coverage. We have fitted equation (1) to the experimental data in the multilayer adsorption range $p/p_0 \leqslant 0.5$ by adjusting ϵ_0 and k as free parameters (the solid line in figure 1(a)). This allows also an extrapolation into the region of capillary condensation, where the multilayer formation cannot be observed directly.

(2) As an approximation, we assume spherically shaped cavities with radius R. Then a sphere with the *reduced radius* $\hat{R} = R - h(p)$ is available for capillary condensation. Subtraction of the *FHH curve* (the solid curve in figure 1(a)) from the desorption branch of the isotherm gives the amount of material n_{cc}, which is desorbed due to the process of capillary (de-)condensation.

(3) When the pressure is reduced during desorption from p_1 to p_2, then $\Delta n_{cc} = n_{cc}(p_2) - n_{cc}(p_1)$ gives the number of adsorbate molecules, desorbed in this particular step due to capillary (de-)condensation. This material stems from pores with radii R in the range $\hat{R}_1 + h(p_1) \leqslant \hat{R}_2 + h(p_2)$, where the $\hat{R}_{1,2}$ are obtained from the *Kelvin equation*:

$$p_{1,2}(R) = p_0 \exp\left(\frac{-2\sigma_{lv} v_L}{k_B T \hat{R}_{1,2}} \right). \tag{3}$$

σ_{lv} is the liquid–vapour surface tension ($\sigma_{lv} = 17.8$ mN m^{-1} at $T = 92.5$ K [19]); v_L is the molar volume of the liquid phase.

(4) The pore size distribution $\rho(r)$ follows from

$$\rho(R) = \frac{(\hat{R} + h(p))^3}{\hat{R}^3} \frac{\Delta n_{cc}\, v_L}{\Delta R} \tag{4}$$

with $\Delta R = R_2 - R_1$. $\rho(R)$ gives the volume, which is accessible to the adsorbate in the form of spherical cavities with radii within the interval ΔR.

Figure 1(b) shows the resulting pore volume distribution. It has a maximum near $R = 55$ Å and a FWHM $\sim$20 Å.

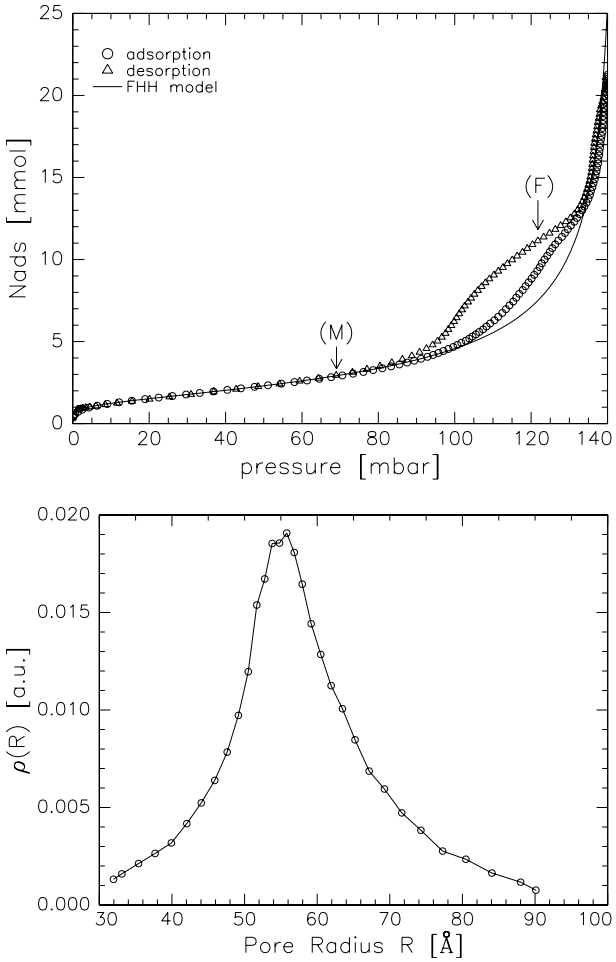

Figure 1. (a) The sorption isotherm of CH_4 in porous TiO_2 at $T = 92$ K. $p_0 = 145$ mbar is the saturation pressure of methane. Adsorption and desorption show a clear hysteresis, which is typical for capillary condensation. (F) and (M) denote the two different fillings (completely filled pores and multilayer coverage, respectively), investigated in the neutron scattering experiments. The solid line describes the multilayer adsorption according to the FHH model (see equation (1)). (b) The pore size distribution extracted from the isotherm according to equation (4).

3. Neutron scattering experiments

The neutron scattering experiments were carried out on the time-of-flight spectrometer IN5, ILL Grenoble, France [8]. A flat aluminium sample cell of thickness 1 mm was used (sample volume 1.08 cm^3). The wavelength of the incoming neutrons was $\lambda = 6.5$ Å for the inelastic measurements at low temperature ($T = 5$ K), and $\lambda = 5$ Å for the quasielastic measurements at higher temperatures between $T = 50$ K and 95 K. The corresponding energy resolutions at the elastic position were determined by using a vanadium standard. On the basis of the isotherm in figure 1, two samples were prepared for the neutron scattering experiments in the following way: the empty TiO_2 substrate was heated up to $T = 275$ K under vacuum in order to remove physisorbed water. It was kept at that temperature for 12 hours (final

pressure $p = 10^{-6}$ mbar). Thereafter the sample was cooled down to $T = 92$ K, where the condensation was performed. The methane was dosed stepwise into the sample cell until the saturation pressure $p_0 = 145$ mbar was reached. Thereafter, in a first desorption step, the pressure was reduced to $p = 0.85\,p_0$ (sample (F)). This removes bulk CH_4, which forms outside the pores and also empties the largest mesopores with radii $R \geqslant 100$ Å. In a second desorption step, the pressure was further reduced to $p = 0.5\,p_0$ (sample (M)). Now only the inner surfaces are covered by a thin film of CH_4 molecules. The nominal thickness of this film is about 5 Å, which means about one monolayer. We will call sample (M) the 'multilayer coverage' according to the usual convention in the literature [1]. A scan with the clean TiO_2 substrate showed elastic scattering from the host material and the sample cell, but no inelastic features. This means that the inelastic/quasielastic scattering is entirely due to the dynamics of the CH_4 molecules. The transmission of the samples was about 90%.

3.1. Inelastic neutron scattering at low temperatures

Figure 2 shows the INS spectrum at $T = 5$ K of CH_4 in TiO_2 with completely filled pores (sample (F)). The scan with the empty host material was subtracted. The most prominent feature is a superposition of two contributions:

(1) excitations at $\hbar\omega = 0.075$ meV, 0.145 meV (tunnelling lines) and 1.08 meV (the free-rotor line) belonging to the partially ordered phase II of bulk methane [20]; and
(2) a broad distribution of excitation energies extending from the tunnelling lines up to the free-rotor line of phase II.

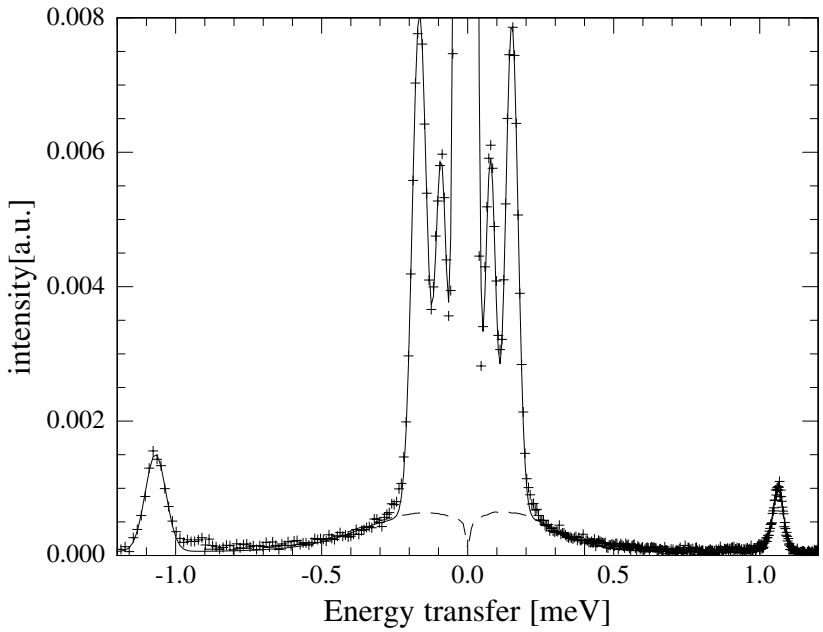

Figure 2. The neutron spectrum of CH_4 in porous TiO_2 ($T = 5$ K; $\lambda = 6.5$ Å) with completely filled mesopores (sample (F)). Visible are the tunnelling lines at $\hbar\omega = 75\ \mu$eV, $\hbar\omega = 145\ \mu$eV and the free-rotor line at $\hbar\omega = 1.08$ meV of CH_4-II. Additionally, a broad distribution of excitation energies shows up below the elastic line, which is described quantitatively (dashed line) by the statistical model explained in the text. The solid line is the sum of the dashed line and Gaussians, which describe the elastic and the inelastic lines.

These latter excitations are attributed to a phase without long-range orientational order, which probably forms near the pore walls. It will be called phase I′ in the following. Very similar spectra were observed with CH_4 condensed in controlled-pore glass with average pore diameter $d = 120$ Å (CPG120) [12]. Surprisingly, also the spectrum of the multilayer coverage (sample (M); see figure 3) contains contributions from phase II in addition to those from phase I′. This is in clear contrast to what has been observed with CH_4 in CPG120, where only scattering from phase I′ occurred at that coverage. As a description of the orientationally disordered phase I′, a model with a Gaussian distribution of tunnel-matrix elements is used. This model is presented in detail in reference [12]; therefore only a brief description is given here: In terms of the pocket state formalism [21] the rotations of a CH_4 tetrahedron are basically characterized by four transition-matrix elements h_i ($i = 1, \ldots, 4$) which correspond to 120° rotations about the four threefold-symmetry axes of the molecule. The strength and symmetry of the orientational potentials acting on the methane molecules in the disordered phase I′ are assumed to be statistically distributed, leading to a corresponding statistical distribution of transition-matrix elements h_i ($i = 1, 2, 3, 4$). A simple assumption is that of a Gaussian distribution with mean value h_0 and width δ:

$$f(h_i) \sim \exp\left(-\frac{(h_i - h_0)^2}{2\delta^2}\right) \qquad i = 1, \ldots, 4. \tag{5}$$

Once a set of four h_i has been selected, the Hamiltonian matrix can be diagonalized, giving the energies of the (in general) fivefold-tunnel-split librational ground state. This procedure is repeated typically 10^6 times and yields the scattered intensity as a function of the energy transfer for a particular set of h_0 and δ (see equation (5)). The contributions from phase I′ in figures 2 and 3 are well described by this model. $V = 17.6(7)$ meV (figure 2) and $V = 18.0(7)$ meV (figure 3) were obtained. These values are about 25% higher than those

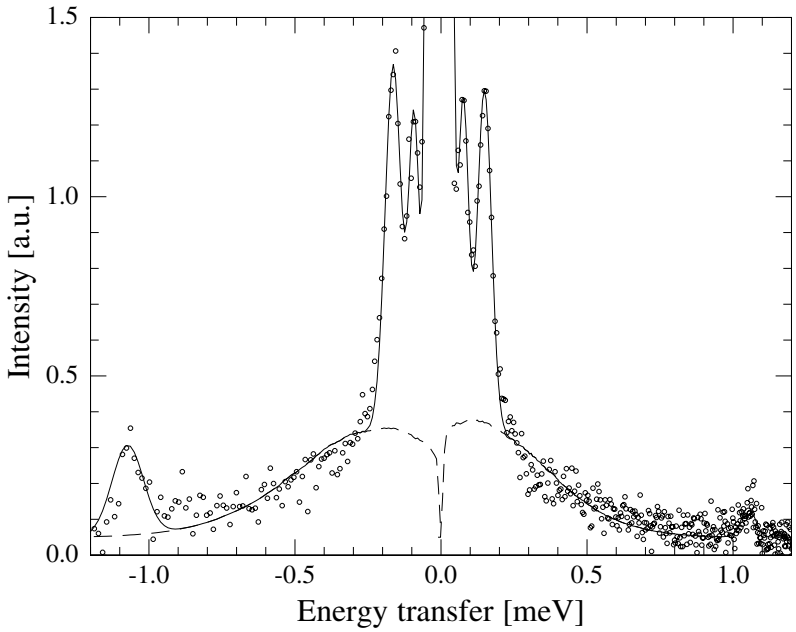

Figure 3. The neutron spectrum of the multilayer coverage (sample (M)) of CH_4 in TiO_2 ($T = 5$ K; $\lambda = 6.5$ Å). The meaning of the dashed and the solid lines is the same as in figure 2.

found for CH_4 in the various SiO_2 modifications [11, 12]. For comparison: $V = 24$ meV is the corresponding value for the ordered molecules in CH_4-II.

Additional information is contained in the dependence of the scattered intensities on momentum transfer Q. The Q-dependence has been calculated by Ozaki *et al* for the rotational transitions of CH_4-II on the basis of an expansion of the potential and wave-function in free-rotor functions [22]. For the $0 \rightarrow 1$ free-rotor transition of CH_4-II at $\hbar\omega = 1.08$ meV, for example, the following expansion in spherical Bessel functions $j_l(Qr)$ was obtained and confirmed experimentally [20]:

$$S_{01}(Q) = 45C\exp(-\gamma Q^2)p_0(T))[0.873j_1^2(Qr) + 0.0581j_3^2(Qr) + 0.0605j_5^2(Qr) + \cdots]. \tag{6}$$

$r = 1.093$ Å is the radius of the methane molecule. $p_0(T)$ denotes the population of the rotational ground state. Equation (6) was fitted to the experimental data for the completely filled pores by adjusting the normalization constant C and $\gamma = 0.02$ Å^2 was used in the Debye–Waller factor. The measurements are in good agreement with the theoretical prediction (see figure 4(a)). The Q-dependence of the scattering from phase I′ is also described by equation (6).

Based on the scattering functions for the inelastic intensities, a prediction can be made for the Q-dependence of the elastic intensity. This is shown in figure 4(b). The solid line in

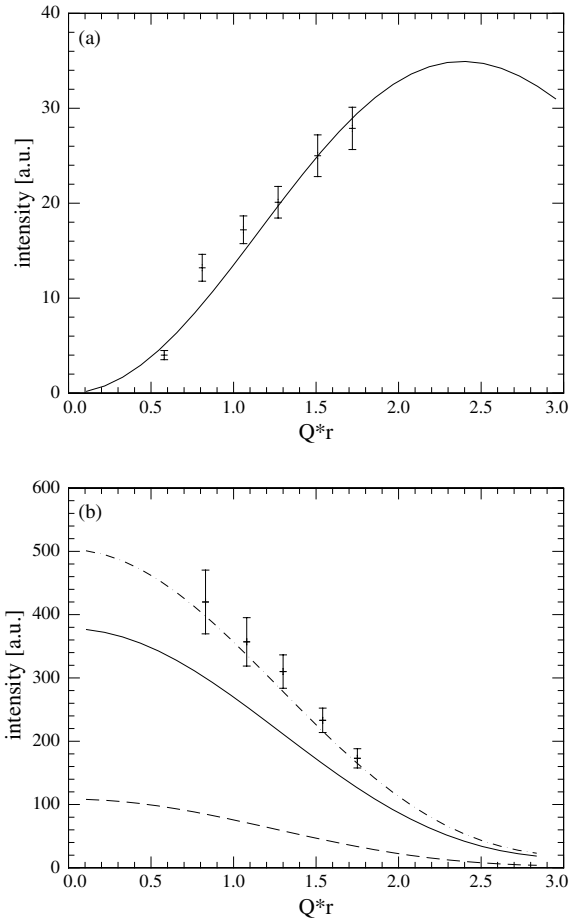

Figure 4. (a) The intensity of the $0 \rightarrow 1$ transition at $\hbar\omega = 1.08$ meV as a function of momentum transfer Q. The solid line refers to the intensity calculated on the basis of the free-rotor model [22]. (b) The elastic intensity; solid line: elastic scattering from phase II; dashed line: scattering from phase I′; dot–dashed line: total elastic scattering.

figure 4(b) is the elastic contribution from molecules of phase II while the dashed line refers to contributions from molecules in phase I′. The sum of the two (dashed–dotted) is in good agreement with experimental values. This means that the elastic intensity is a direct measure for the number of molecules in the two phases: about 80% belong to phase II and 20% belong to phase I′. Assuming that phase I′ forms a thin film on the pore walls and that the mesopores have spherical shape with average radius $\bar{R} = 55$ Å, a film thickness of $d \sim 5$ Å follows. This indicates that a monomolecular film is adsorbed on the inner surfaces and that the disordering influence of the walls is restricted to this film.

The reason for the existence of phase II in sample (M) (multilayer coverage) is as yet unclear. Even in the case of smooth walls (for example CH_4 on MgO surfaces [13]) at least four layers of methane molecules are needed to obtain the spectrum of phase II. We will discuss this point in section 5.

3.2. Quasielastic neutron scattering at high temperatures

The quasielastic neutron scattering measurements were performed on the same samples as were used for the inelastic measurements. The measurements covered the temperature range from $T = 50$ K up to $T = 94$ K, with the wavelength $\lambda = 5$ Å of the incoming neutrons. For the completely filled mesopores (sample (F)) the QENS spectra were taken both on cooling and on heating. In the multilayer regime (sample (M)) the QENS spectra were measured during cooling only. Spectra at three temperatures ($T = 75$ K, 85 K, and 94 K) are shown in figure 5. At the lowest temperature, a broad, but relatively weak quasielastic distribution occurs due to rotational diffusion of the CH_4 molecules.

With increasing temperature the quasielastic component grows strongly at the expense of the elastic intensity. This indicates melting of methane condensates in the mesopores. For both samples, we have found a broad temperature range where a satisfactory description of the scattered intensities was only possible with the assumption of contributions from both a liquid and a solid phase. In the following, we describe how the quantitative information (i.e. diffusion constants, fraction x of the scatterers in the liquid phase) was extracted from the spectra. The interpretation follows in section 4.

3.3. The model

It is assumed that a fraction $x(T)$ of the molecules are in the liquid phase, performing rotational and translational diffusion, and that a fraction $(1 - x(T))$ of the molecules are in the solid phase with rotational diffusion only. Under the assumption of an uncorrelated superposition of rotational and translational motion in the liquid phase, the scattering function contains two components:

$$S(Q, \omega) = (1 - x(T))S_{rot}(Q, \omega) + x(T)S_{rot}(Q, \omega) \otimes S_{trans}(Q, \omega). \tag{7}$$

$S_{rot}(Q, \omega)$ is the scattering function for rotational diffusion of molecules in the solid and liquid phases. $S_{trans}(Q, \omega)$ is the scattering function for translational diffusion in the liquid phase, which has to be convoluted with $S_{rot}(Q, \omega)$.

The scattering functions may be written as (see [3] for details)

$$S_{rot}(Q, \omega) = A_0(Qr)\delta(\omega) + \sum_{l=1}^{\infty} A_l(Q)L(\omega, D_{rot}l(l+1)) \tag{8}$$

$$S_{rot}(Q, \omega) \otimes S_{trans}(Q, \omega) = \sum_{l=0}^{\infty} A_l(Qr)L(\omega, \Gamma_l) \tag{9}$$

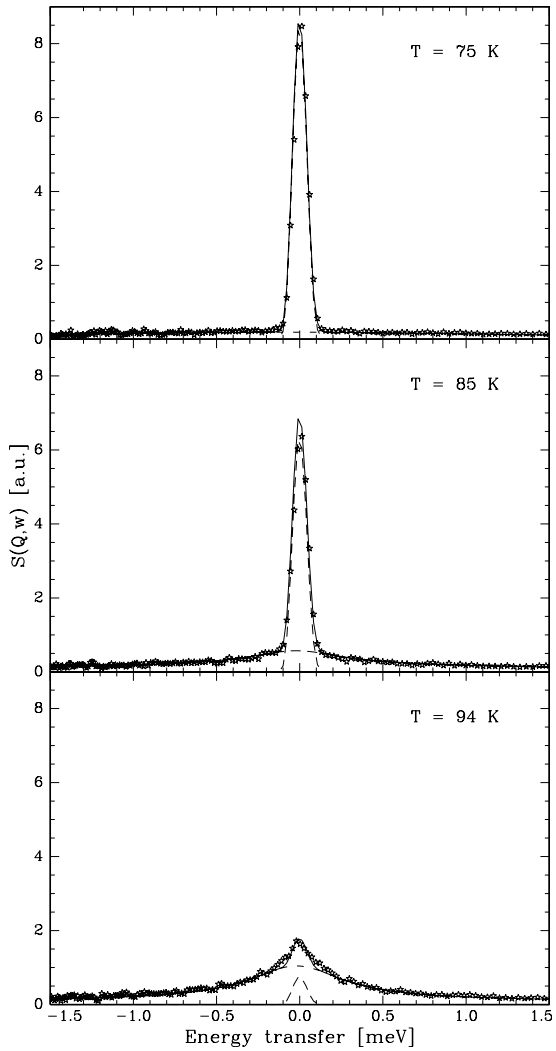

Figure 5. Quasielastic neutron spectra ($\lambda = 5$ Å, $Q = 1.32$ Å^{-1} for CH_4) in the mesopores of TiO_2 at three temperatures. Clearly visible is the decrease of the elastic intensity and the increase of the quasielastic scattering with increasing temperature. The upper spectrum corresponds to a completely solid condensate (rotational diffusion) and the lower spectrum to the liquid condensate (rotational and translational diffusion).

with

$$\Gamma_l(Q,T) = D_{trans}Q^2 + D_{rot}l(l+1)$$
$$A_l(Qr) = (2l+1)(j_l(Qr))^2.$$

Here $L(\omega,\Gamma)$ is a Lorentzian of width Γ. $D_{rot}(T)$ denotes the rotational diffusion constant. $D_{trans}(T)$ is the translational diffusion constant in the liquid phase.

$$A_0(Q,r) = (\sin(Qr)/Qr))^2 \tag{10}$$

in equation (8) is the elastic incoherent structure factor (EISF) of the scattering from the solid phase (see equation (9)).

In a first step of the data analysis, scattering functions with different D_{rot} for the solid and liquid phases were used. Since, however, almost identical numerical values for the diffusion constants were obtained, in the following identical functions $S_{rot}(Q, \omega)$ for the liquid and the solid phases were used.

The scattering functions in equations (8)–(10) are the Fourier transforms of the solutions of Fokker–Planck equations for diffusional (translational and rotational) motions. The translational contribution to the linewidth in equation (10) has the Q^2-dependence of a simple (translational) diffusive motion. For details see [3].

3.4. Application of the model

The spectra from the single detectors were grouped together for intensity reasons to yield seven sum spectra with average momentum transfers at the elastic positions of $Q = 0.35$ Å^{-1}, 0.75 Å^{-1}, 1.0 Å^{-1}, 1.3 Å^{-1}, 1.5 Å^{-1}, 1.8 Å^{-1}, 2.1 Å^{-1}. For each temperature, the scattering function $S(Q, \omega)$ from equation (7) was convoluted with the energy resolution function of the spectrometer and fitted to the seven sum spectra simultaneously. The free parameters were the diffusion constants D_{rot}, D_{trans}, and the fraction $x(T)$ of molecules in the liquid phase. Additionally, a Debye–Waller factor was included.

Figure 6 shows as an example the fit for $T = 94$ K and three different Q-values. The temperature dependence of the fraction $x(T)$ of molecules in the liquid phase is displayed in figure 7.

For the completely filled pores, x increases with increasing temperature from very small values up to values $x \simeq 1$ within a temperature range $\delta T \simeq 10$ K. A hysteresis loop of $\delta T = 5$ K was observed. For the multilayer coverage, the increase of x is smeared out over a temperature range $\Delta T \simeq 20$ K, and x is significantly smaller than unity even for the highest temperature $T = 93$ K.

For both samples investigated, the diffusion constants display an Arrhenius behaviour (figure 8). We have derived an activation energy $E_a = 13.0(8)$ meV for the translational diffusion constants for the completely filled mesopores, and $E_a = 14.0(8)$ meV in the multilayer regime.

The activation energies for the rotational diffusion constants are $E_a = 5.4(5)$ meV (sample (F)) and $E_a = 6.2(5)$ meV (sample (M)). For comparison, a value $D_{trans} = 2.5 \times 10^{-5}$ cm^2 s^{-1} is reported in reference [23] for liquid methane at $T = 95$ K. In our case, the translational diffusion constants are considerably smaller. Our results also show that the diffusion constants in the multilayer sample are slightly smaller then for the completely filled pores, indicating a slower dynamics of the CH_4 molecules on the inner surfaces.

4. Melting of the condensate in the mesopores

In our approach, to describe the freezing behaviour of the CH_4 condensate with decreasing temperature in the mesopores, we have applied the *two-phase model* of Hill [7], which assumes that the system under consideration (here the condensate in a specific pore with radius R) is in one of two possible states (i.e. the condensate is either completely liquid or it is completely frozen). For constant volume V and constant chemical potential μ, the probability of finding the condensate in the liquid state is

$$P_L(R, T) = \exp\left(-\frac{\Delta J}{k_B T}\right) \Big/ \left[1 + \exp\left(-\frac{\Delta J}{k_B T}\right)\right] \tag{11}$$

$$\Delta J = J_L - J_S \tag{12}$$

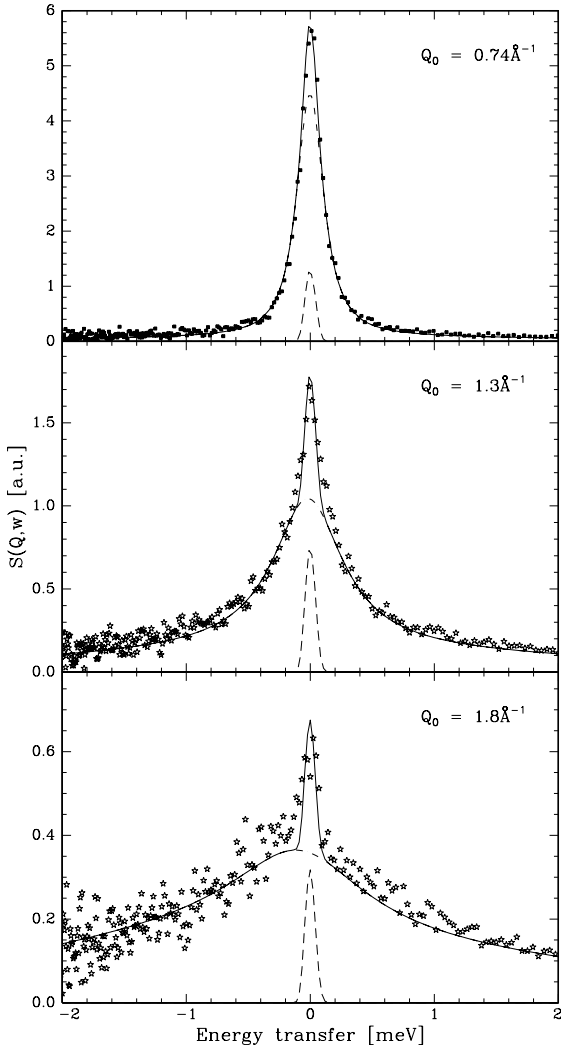

Figure 6. The Q-dependence of the intensities at $T = 94$ K (completely filled pores). The solid line corresponds to the model explained in the text. The dashed line is the elastic component.

where J_L is the grand canonical potential for the system in the liquid state and J_S that for the system in the solid state.

At a temperature T, the fraction of CH_4 molecules in the liquid phase may be calculated from the pore volume distribution $\rho(R)$:

$$x_L(T) = \frac{1}{v_L}\int_0^{r_{max}} \rho(R) P_L(R, T)\, \mathrm{d}R. \tag{13}$$

r_{max} is the radius of the largest pores, which remained filled after the desorption steps during the sample preparation (see section 2). It is assumed that for completely filled pores, ΔJ consists of a volume contribution with a temperature dependence proportional to $\Delta T = T_m - T$ ($T_m = 91$ K is the bulk melting point of methane) and a surface contribution, which is temperature independent:

$$\Delta J = C_1 \frac{\Delta T}{T_m} R^3 + C_2 R^2. \tag{14}$$

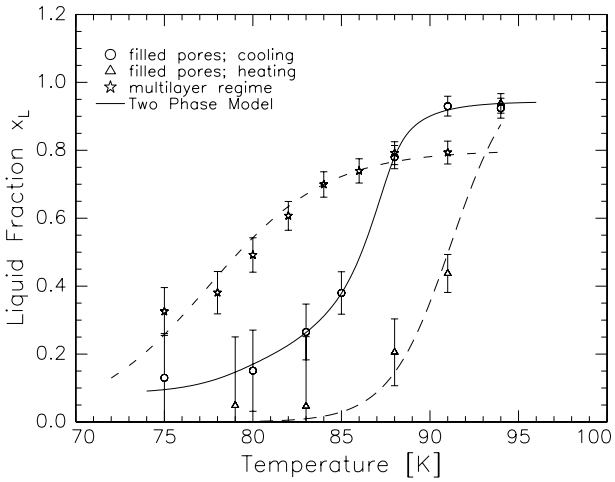

Figure 7. The temperature dependence of the concentration x_L of the liquid phase. Shown are the experimental values for the completely filled pores (obtained both on cooling and on heating) and for the multilayer coverage. The solid line represents a description by the *two-phase model*, while the dashed lines are guides to the eyes only.

C_2 is closely related to the surface tension of the methane crystallites:

$$C_2 = 4\pi(\sigma_{wl} - \sigma_{ws}) = 4\pi\ \Delta\sigma. \tag{15}$$

σ_{wl} and σ_{ws} are the liquid–wall and the solid–wall surface tensions, respectively (more accurately: the surface tensions of the interface between the condensate and the amorphous CH_4 multilayer on the pore walls). As pointed out by Awschalom and Warnock [25], $\Delta\sigma$ might change during the freezing process, because the freezing front may propagate partially through the multilayer after the liquid in the centre of the pore is frozen. This might also account for the hysteresis between melting and freezing.

The following analysis assumes that 20% of the methane molecules (namely those in the multilayer) show the melting behaviour according to the multilayer branch in figure 7, while the liquid/solid transition of the remaining 80% may be described by equation (13). Under these two assumptions, the solid line in figure 7 was obtained by adjusting C_1 and C_2 in equation (14). The resulting numerical value for $\Delta\sigma$ indicated a relatively small change (about 5%) in the surface tension, when the condensate freezes. Such a small difference in the surface tensions is not surprising, if one recalls that it is actually the surface tension between the condensate and the (highly viscous) multilayer film on the inner surface.

5. Summary and conclusions

On the basis of the sorption isotherm, two different degrees of pore filling were realized (completely filled pores and inner walls covered). In both cases, however we found the coexistence of phase II (the low-temperature phase of unperturbed methane) with phase I′ (no long-range orientational ordering of the CH_4 tetrahedra) in the inelastic spectra at $T = 5$ K. Assuming that phase I′ forms as a thin film on the walls of spherical pores with radius $R = 55$ Å, a nominal film thickness of $d \sim 5$ Å was calculated, which would correspond to a monomolecular CH_4 layer. This coexistence was also found for CH_4 in the mesopores of controlled-pore glass (average pore diameter $d \sim 120$ Å; filled pores), but with considerably different relative intensities of the two phases [12]. It is quite unrealistic to assume that the disordering influence of the pore walls should be restricted to the first layer of methane molecules. Additionally, the occurrence of scattering from phase II in the multilayer sample (sample (M)) shows that even there larger CH_4 crystallites must be present. Both findings

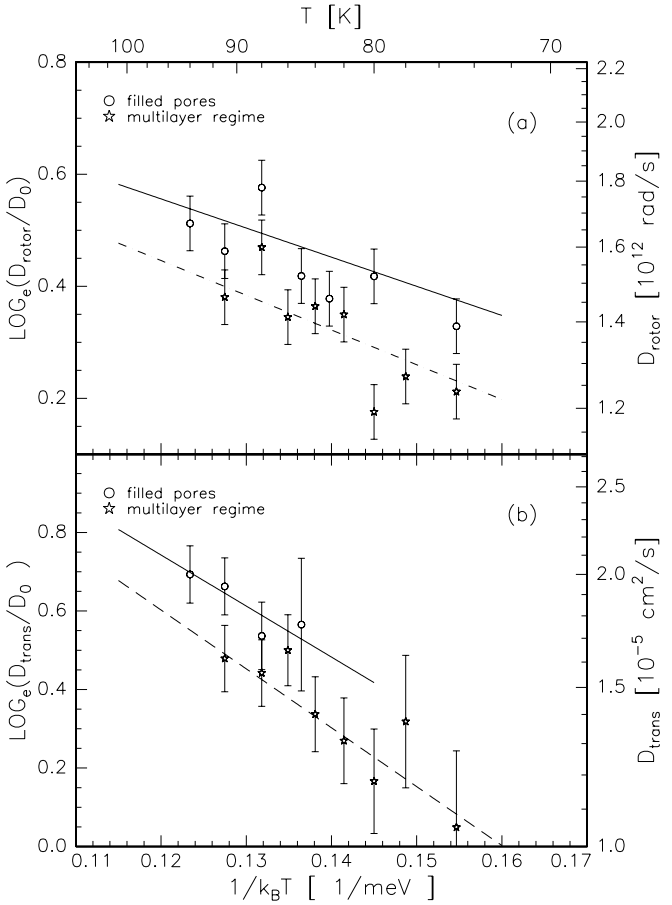

Figure 8. Arrhenius plots of the diffusion constants: (a) rotational diffusion constants; activation energy $E_a = 6$ meV for both curves; (b) translational diffusion constants; activation energy $E_a = 12$ meV for the completely filled pores (lower curve) and $E_a = 14$ meV in the multilayer regime (upper curve).

might be indicative of the existence of larger crystallites outside the pores. On the other hand, the adsorption/desorption procedure described in section 2 excludes the possibility that these crystallites have already formed during the sample preparation. One possible explanation is that a partial dewetting could take place upon cooling, which would lead to the formation of CH_4 crystallites (possibly larger than those in the mesopores) outside the pores.

In the intermediate temperature range around $T = 50$ K, the dynamics of the methane molecules is characterized by pure rotational diffusion. The rotational diffusion constant displays an Arrhenius behaviour with an activation energy $E_a = 6$ meV.

The quasielastic spectra in the melting region of the condensate could be explained by the coexistence of a liquid phase (rotation + translation; concentration x) with a solid phase (pure rotation; concentration $1 - x$). For the completely filled pores, x increases with increasing temperature from very small values up to values $x \simeq 1$ within a temperature range $\delta T \simeq 10$ K. A clear hysteresis was observed.

For the multilayer coverage the increase of x is smeared out over a temperature range larger than 10 K, and x is still smaller than 1 for the highest temperature $T = 93$ K. The Monte Carlo

simulations of Miahara and Gubbins [26] for CH_4 on graphite have shown that the freezing temperature of the contact layer depends sensitively on both the adsorbate–substrate and the adsorbate–adsorbate interactions, and that a decrease of T_m might occur as well as an increase. The translational diffusion constants show Arrhenius behaviour. The activation energies are $E_a = 12$ meV for filled pores and $E_a = 14$ meV for the multilayer coverage.

The temperature dependence of the fraction of molecules in the liquid phase can be described by the simple *two-phase model* of Hill [7], which assumes a *barrier* ΔJ to be crossed by the condensate in a pore, when undergoing the liquid–solid transition. This barrier ΔJ has a volume and a surface contribution. In this model, no coexistence of liquid and solid phases in the same pore is assumed. The numerical results indicate that only a small increase (about 5%) of the surface tension occurs at the liquid $\rightarrow$ solid transition of the condensate. This small difference can be understood at least qualitatively from the fact that it is actually not the surface tension between the solid or liquid condensate and the wall but the surface tension of the CH_4-condensate/CH_4-multilayer interface which influences the melting temperature.

Acknowledgments

The authors would like to thank K Rahattalab for his support during the isotherm measurements. This work was supported by the *Deutsche Forschungsgemeinschaft* under project No PR325/7-1.

References

[1] Adamson A W 1990 *Physical Chemistry of Surfaces* (New York: Wiley)
[2] Brunauer S 1945 *The Adsorption of Gases and Vapors* vol 1 (Princeton, NJ: Princeton University Press)
[3] Bee M 1988 *Quasielastic Neutron Scattering* (Bristol: Hilger)
[4] Wells A F 1975 *Structural Inorganic Chemistry* (Oxford: Clarendon)
[5] Frenkel Y P 1955 *Kinetic Theory of Liquids* (New York: Dover)
[6] Hadjivanov K I and Klissurski D K 1996 *Chem. Soc. Rev.* **25** 61
[7] Hill T L 1963 *Thermodynamics of Small Systems* (New York: Benjamin)
[8] Ibel K (ed) 1994 *The Yellow Book; Guide to Neutron Research Facilities at the ILL* (Grenoble: ILL)
[9] Kresge C T, Leonowicz M E, Roth W J, Vartuli J C and Beck J S 1992 *Nature* **359** 710
[10] Bellissent-Funel M C, Chen S H and Zanotti J M 1995 *Phys. Rev.* E **51** 4558
[11] Balszunat D, Asmussen B, Coddens G and Ferrand M 1996 *Physica* B **226** 184
[12] Gutt C, Asmussen B, Krasnov I, Press W, Langel W and Kahn R 1999 *Phys. Rev.* B **57** 8607
[13] Larese J 1995 private communication
[14] Morishige K and Nobuoka K 1997 *J. Chem. Phys.* **107** 6965
[15] Pfeifer P 1988 *Fractals in Surface Science: Scattering and Thermodynamics of Adsorbed Films (Springer Series in Surface Science vol 10)* ed R Vanselow and R Howe (Berlin: Springer)
[16] Schäfer B 1998 *PhD Thesis* University of Siegen
[17] Sing K S W, Everett D H, Haul R A W, Moscou L, Pierotti R A, Rouqverol J and Siemeniwska T 1985 *Pure Appl. Chem.* **57** 603
[18] Sokol P E, Azuah R T, Gibbs M R and Bennington S M 1996 *J. Low Temp. Phys.* **103** 23
[19] Beaton C F and Hewitt G F 1989 *Physical Property Data for the Design Engineer* (New York: Taylor and Francis)
[20] Asmussen B, Prager M, Press W, Blank H and Carlile C J 1992 *J. Chem. Phys.* **97** 1332
[21] Hüller A 1977 *Phys. Rev.* B **16** 1844
[22] Ozaki Y, Kataoka Y and Yamamoto T 1980 *J. Chem. Phys.* **73** 3442
[23] Oosting P H and Trappenings N J 1971 *Physica* **51** 418
[24] Thorel P, Coulomb J P and Bienfait M 1981 *J. Physique* **42** 293
[25] Awschalom D D and Warnock J 1987 *Phys. Rev.* B **35** 6779
[26] Miahara M and Gubbins K E 1997 *J. Chem. Phys.* **106** 2865